APPLICATION TO SYNTHETIC DATA

We ~~test the proposed method by applying it~~ to three ~~different~~ synthetic data sets simulating ~~complex~~ geological scenarios. The first one is generated by a model containing ~~a set of~~ sources with different geometries, all of them with the same magnetization direction. The second data set is generated by ~~a set of~~ magnetized bodies~~, but one them is~~ a shallow ~~interfering~~ source with the same magnetization direction. In the third test, we violate the unidirectional ~~approach~~ by simulating ~~an interfering~~ shallow source with different magnetization direction from the ~~others~~ bodies.

~~For~~ all tests, the simulated data were computed on ~~an irregular~~ grid of 49×25 points (a total of $N = 1225$ observations) at a constant height of $100\,m$. We assume an observation area ~~of~~ extending $12\,km$ along the x- and y-axis, resulting a grid spacing of $250\,m$ and $500\,m$ on x- and y-~~axis~~, respectively. The data were contamined with pseudorandom Gaussian noise with zero mean and $10\,nT$ standard deviation. The main ~~field~~ direction simulated was $I = -40°$ and $D = -22°$ for the inclination and declination, respectively. ~~For~~ the inversion, we use an equivalent layer composed by a grid of 49×25 dipoles (a total of $M = 1225$ equivalent sources) positioned at a depth of $z_c = 1150\,m$ below the observation plane (2.5 times the greater grid spacing). We use the L-curve to choose the regularizing parameter (μ). ~~The~~ algorithm ~~1~~ starts with an initial guess $\mathbf{q}_0 = (-10°, -10°)$ for inclination and declination, respectively.

Unidirectional magnetization ~~direction~~ sources

~~In order to test the methodology, we~~ generate a 3D prism with polygonal cross-section whose the top is positioned at a depth of $450\,m$ and the bottom $3150\,m$ with magnetization

intensity of $4\,A/m$. We also generate two spheres with radius equal to $500\,m$, one of them with the coordinates of center $x_c = 1800\,m$, $y_c = -1800\,m$ and $z_c = 1000\,m$ and the other with $x_c = 800\,m$, $y_c = 800\,m$ and $z_c = 1000\,m$. The magnetization intensity for the two both spheres is equal to $3\,A/m$. We produce two rectangular prisms with the same $2.5\,A/m$ of magnetization intensity. The smaller prism has the top at a depth of $450\,m$ and side lengths of $1000\,m$, $700\,m$ and $500\,m$ along x-,y- and z-axis, respectively. The greater prism has the top at a depth of $500\,m$ and side lengths of $1000\,m$, $2000\,m$ and $1550\,m$ along x-,y- and z-axis. All simulated sources have inclination $-25°$ and declination $30°$. The noise-corrupted data is shown in figure 3a.

Figure 3b shows the predicted data produced by equivalent layer. Figure 3c shows the residuals defined as the difference between the simulated data (figure 3a) and the predicted data (figure 3b). The residuals appear normally distributed with a mean of $-0.30\,nT$ and a standard deviation of $9.67\,nT$ as shown in figure 3d. The estimated magnetization direction $\mathbf{q}^\sharp$ has inclination $-28.6°$ and declination $30.8°$. Figure 3e shows the estimated magnetic-moment distribution $\mathbf{p}^\sharp$. The convergence of the algorithm 1 is shown in figure 3f. These results show that the all-positive magnetic-moment distribution and the estimated magnetization direction produce an acceptable data fitting.

Unidirectional model with shallow interfering source

In this section we test the methodology perfomance when exist a shallow interfering source. The model is almost the same as the previous section except the smaller prism. For this purpose, we put the top of the smaller prism at a depth of $150\,m$ and side lengths of $1000\,m$, $700\,m$ and $500\,m$ along x-,y- and z-axis, respectively. The magnetization intensity for this

prism is equal to $1.5\,A/m$. The magnetization direction of all sources is $-25°$ inclination and declination $30°$, respectively. The synthetic data is shown in figure 4a.

Figure 4b shows the predicted total-field anomaly produced by equivalent layer. Figure 4c shows the residuals defined as the difference between the simulated data (figure 4a) and the predicted data (figure 4b). The residuals appear normally distributed with a mean of $-0.42\,nT$ and a standard deviation of $10.67\,nT$ as shown in figure 4d. ~~The estimated magnetization direction $\mathbf{q}^\sharp$ has inclination $-28.7°$ and declination $31.7°$.~~ Figure 4e shows the estimated magnetic-moment distribution $\mathbf{p}^\sharp$. The convergence of the algorithm ~~1~~ is shown in figure 4f. Despite the residual located above the ~~shallow magnetic~~ source, we consider the methodology produced a reliable result. ~~Therefore, that the~~ all-positive magnetic-moment distribution ~~and the estimated magnetization direction~~ produce an acceptable data fitting.

Shallow source with different magnetization direction

In this test we simulate the presence of a shallow ~~interfering~~ body with different magnetization direction from the other magnetic sources. The shallow prism has the dimension, the ~~intensity~~ magnetization ~~and magnetization direction~~ ~~are~~ equal to the previous ~~section~~. However, the magnetization direction of the shallow prism is $20°$ inclination and declination $-30°$. The noise-corrupted data is shown in figure 5a.

Figure 5b shows the predicted total-field anomaly. Figure 5c shows the residuals defined as the difference between the simulated data (figure 5a) and the predicted data (figure 5b). The residuals have a mean of $-0.71\,nT$ and a standard deviation of $10.67\,nT$ as shown in figure 5d. The estimated magnetization direction $\mathbf{q}^\sharp$ has inclination $-30.4°$ and declination $27.6°$. Figure 5e shows the estimated magnetic-moment distribution $\mathbf{p}^\sharp$. The convergence

of the algorithm ~~1~~ is shown in figure 5f. Despite the slight difference ~~for the~~ magnetization direction, the estimated magnetic-moment distribution produces an acceptable data fit. ~~Another feature we can highlight is the data misfit just above the shallow prism with different magnetization direction.~~

APPLICATION TO FIELD DATA

The Goias alkaline province (GAP) is a region in the central part of Brazil that there are occurences of mafic-ultramafic alkaline magmatism. This region presents a variety of rocks with an extense petrographic types. Throughout the area there are mafic-~~ultramagic~~ complexes (plutonic intrusions), subvolcaninc alkaline intrusions (diatremes) and volcanic products (kamafugite lava flows) with several dikes. ~~Among~~ the main alkaline complexes of GAP are ~~the~~ Montes Claros de Goias, Diorama, Corrego dos Bois, Morro do Macaco and Fazenda Buriti. These alkaline intrusions are sorrounded by a Precambrian basement and the Phanerozoic sedimentary rocks of the ~~Paran basin.~~ (Junqueira-Brod et al., 2005; Carlson et al., 2007; Marangoni and Mantovani, 2013; Dutra et al., 2014). Recent studies indicate the existence of a remarkable remanent magnetization component within these intrusions (Marangoni and Mantovani, 2013; Oliveira Jr et al., 2015; Marangoni et al., 2016; Zhang et al., 2018).

~~This area was the target of an~~ aeromagnetic survey ~~with a financial support from the government of the state of Goias (LASA Prospection and Engineer, 2004). This survey~~ has a flight pattern with ~~North-South~~ spaced from $\sim 500\,m$ and $\sim 8\,m$ along each line, and a constant height of $100\,m$ from the terrain. The main field direction for this area was $-19.5°$ and $-18.5°$ for inclination and declination, respectively. ~~In order to test the methodology on a field data, we~~ invert the ~~data~~ from the alkaline complex of Montes Claros. To speed up data processing and inversion, we downsampled the data along the flight lines, resulting a grid of 55×32 points (a total of $N = 1787$ observations). This new set up results an approximately $320\,m$ and $470\,m$ grid spacing along the x- and y-~~axis~~, respectively. ~~Figure 6a shows the observed data from the complex of Montes Claros. For the inversion, we~~ use

an equivalent layer composed by a grid of 55×32 dipoles (a total of $M = 1787$ equivalent sources) positioned at a depth of $840\,m$ below the observation plane (~ 2 times the greater grid spacing). The algorithm ~~1~~ starts with an initial guess of $-70°$ and $50°$ for the inclination and declination, respectively. Figure 6b shows the predicted data produced by equivalent layer. Figure 6c shows the residuals defined as the difference between the observed data (figure 6a) and the predicted data (figure 6b). ~~The~~ histogram of residuals (figure 6d) ~~presents a~~ mean of $-14.52\,nT$ ($\sim 0.1\%$ of the maximum value of total-field anomaly data) and standard deviation of $312.28\,nT$ ($\sim 2\%$ of the maximum value of total-field anomaly data). The estimated magnetization direction $\mathbf{q}^\sharp$ has inclination $-50.2°$ and declination $34.9°$. Figure 6e shows the estimated magnetic-moment distribution $\mathbf{p}^\sharp$. ~~The~~ convergence of the algorithm ~~1 is shown in figure 6f~~. We check the quality of the estimated magnetization direction by computing the reduction-to-pole of the observed total-field anomaly. ~~Figure 7 shows the RTP anomaly.~~ ~~As we~~ can notice ~~from this last figure is~~ that the RTP ~~field~~ exhibits predominantly positive values and decays to zero towards the borders of study area. For this reason, we consider that the estimated magnetization direction led to a satisfactory RTP anomaly. We conclude with these results that the all-positive magnetic moment distribution and the estimated magnetization direction produce an acceptable data fitting. The estimated magnetization direction also confirms the existence of remarkable remanent magnetization ~~for these instrusions~~.

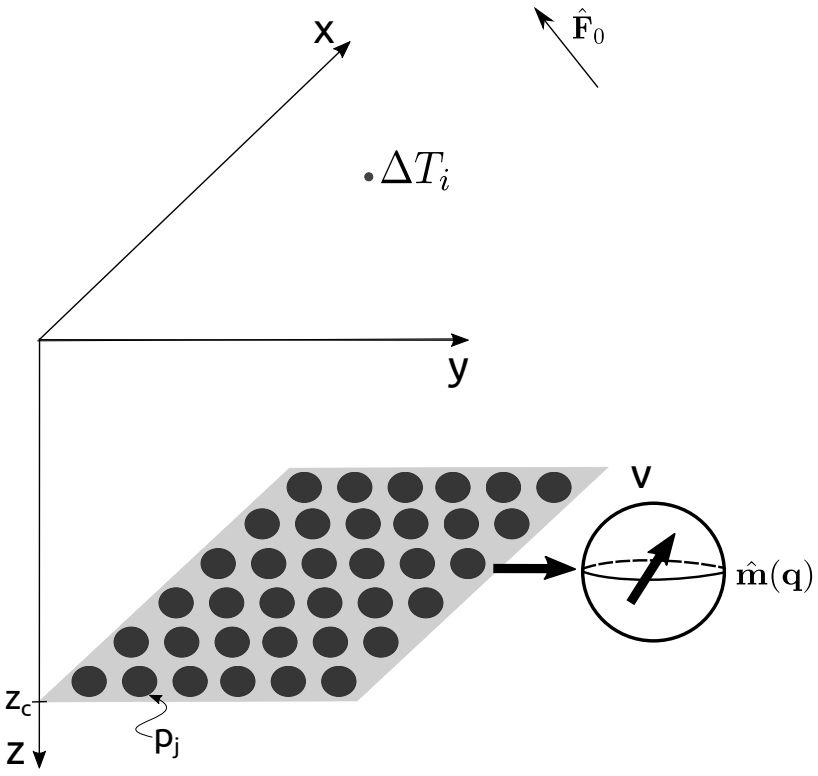

Figure 1: Schematic representation of an equivalent layer. The layer is positioned over the horizontal plane at a depth of $z = z_c$. $\Delta T_i = f_i(\mathbf{s})$ is the predicted total-field anomaly at the point (x_i, y_i, z_i) produced by the set of M equivalent sources (black dots). Each source is located at the point (x_j, y_j, z_c), $j = 1, \ldots, M$, and represented by a dipole with unity volume υ with magnetization direction $\hat{\mathbf{m}}(\mathbf{q})$ and magnetic moment p_j.

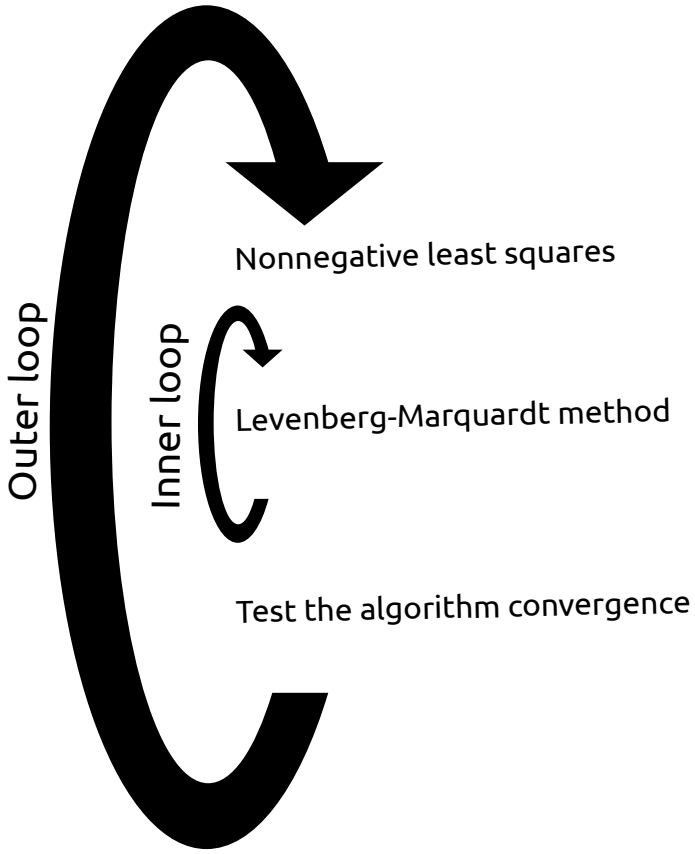

Figure 2: Iterative scheme overview for NNLS and Levenberg-Marquardt method for estimating magnetization direction. The outer loop is the nonnegative solution for magnetic-moment distribution and the inner loop calculates the magnetization direction correction using Levenberg-Marquardt method.

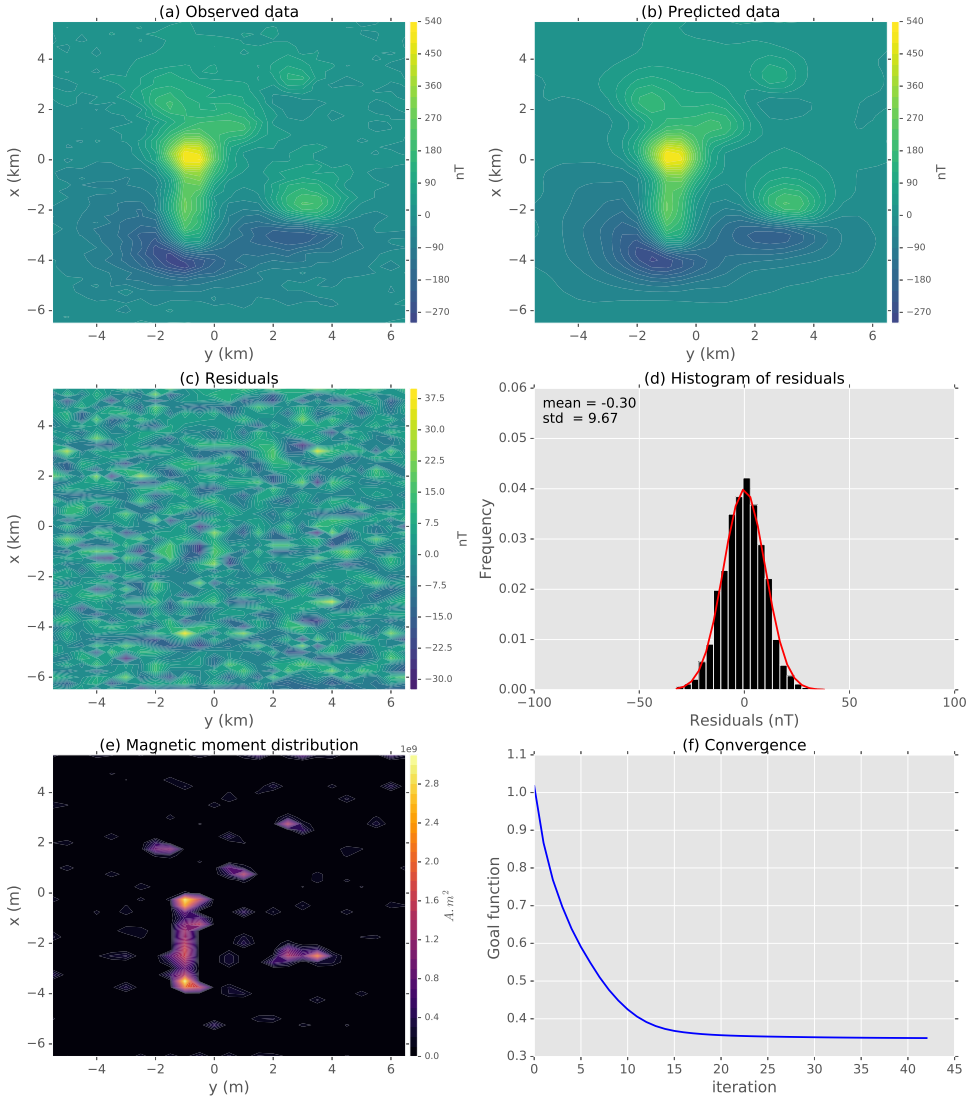

Figure 3: ~~Application to synthetic data for~~ unidirectional ~~model.~~ (a) Noise-corrupted data. (b) Predicted data produced by equivalent layer. (c) Difference between the data shown in panels ~~(a) and (b).~~ (d) Histogram of residuals. (e) All-positive magnetic moment distribution. (f) Goal function value (equation 19a) per iteration showing the convergence.

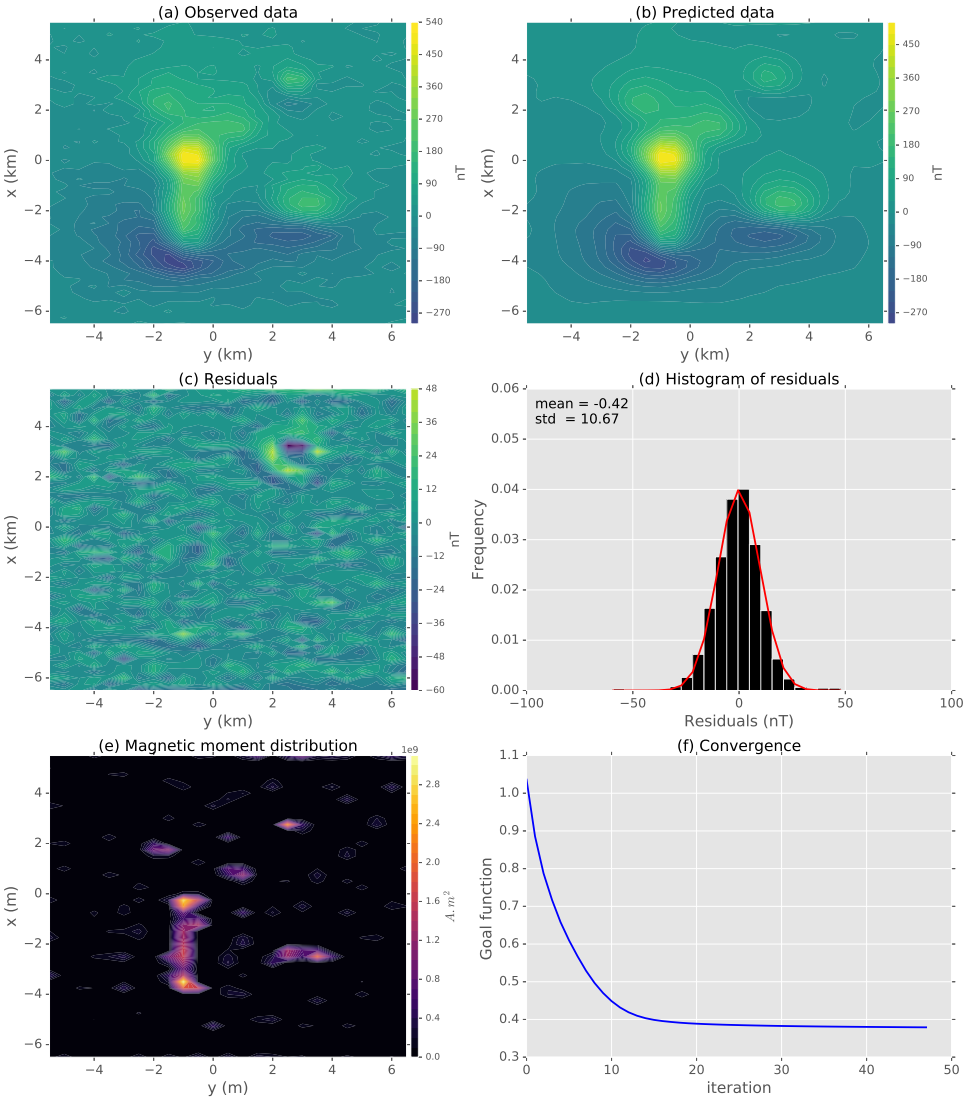

Figure 4: ~~Application to synthetic data with a shallow interfering source.~~ (a) Noise-corrupted ~~data~~. (b) Predicted data produced by equivalent layer. (c) Difference between the data shown in panels ~~(a) and (b)~~. (d) Histogram of residuals. (e) All-positive magnetic moment distribution. (f) Goal function value (equation 19a) per iteration showing the convergence.

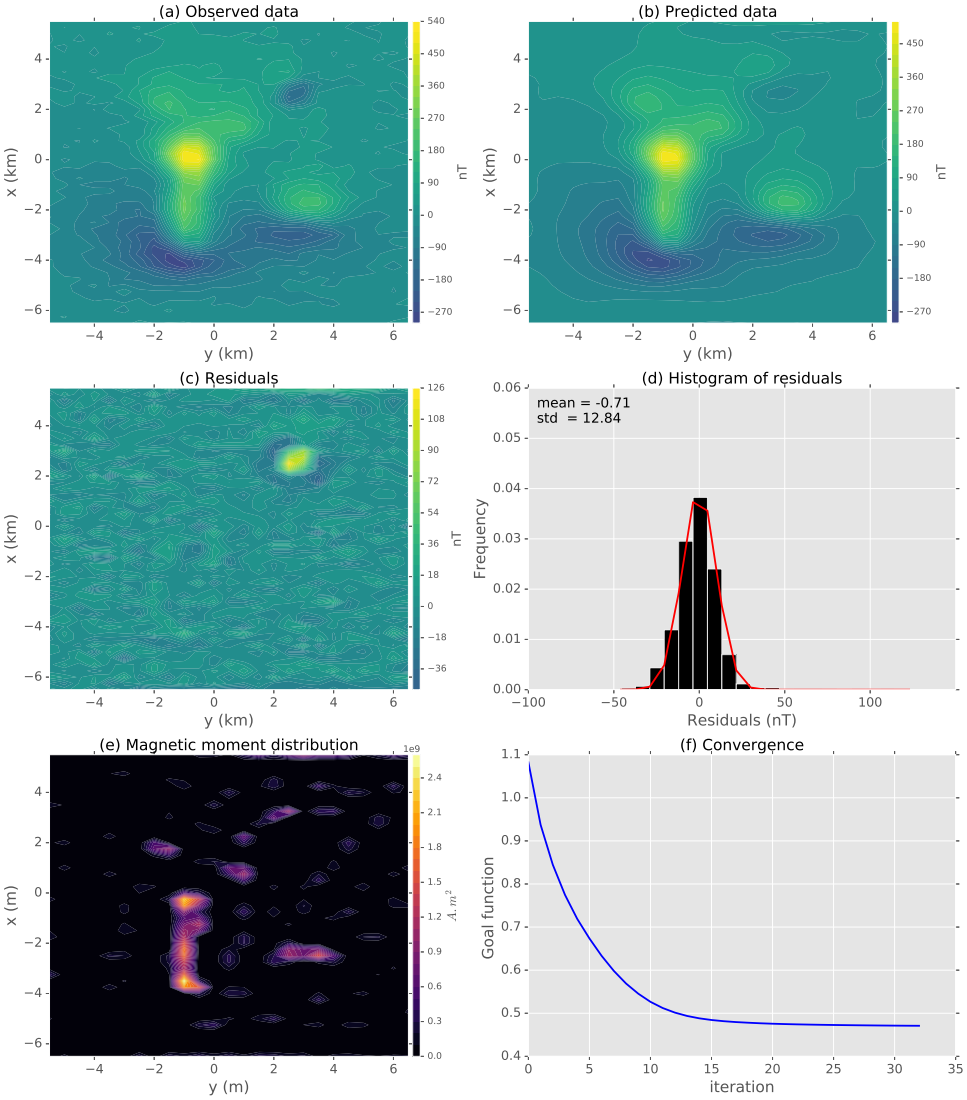

Figure 5: ~~Application to synthetic data with a shallow interfering source with different magnetization direction.~~ (a) Noise-corrupted ~~data.~~ (b) Predicted data produced by equivalent layer. (c) Difference between the data shown in panels ~~(a) and (b).~~ (d) Histogram of residuals. (e) All-positive magnetic moment distribution. (f) Goal function value (equation 19a) per iteration showing the convergence.

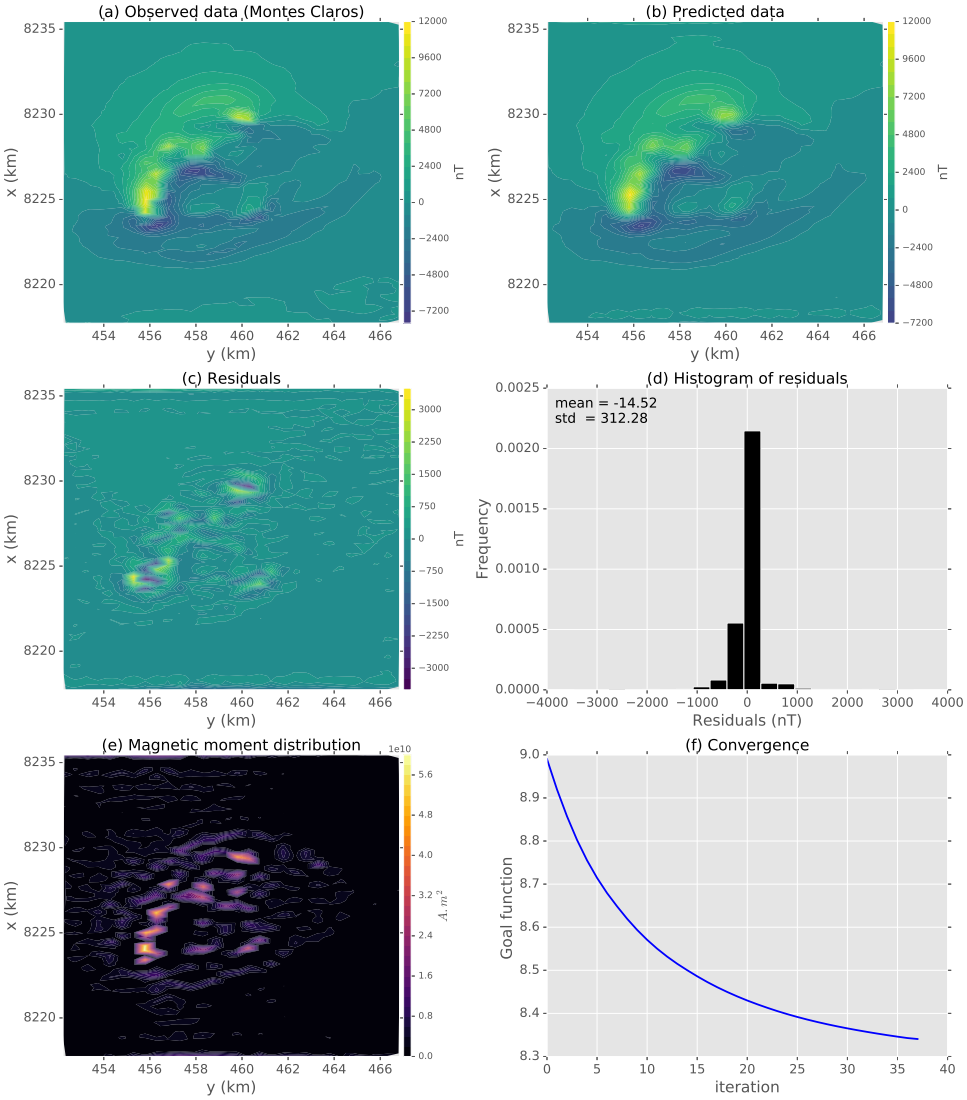

Figure 6: Application to field data ~~located in complex of~~ Montes Claros. (a) ~~Observation data.~~ (b) Predicted data produced by equivalent layer. (c) Difference between the data shown in panels ~~(a) and (b).~~ (d) Histogram of residuals. (e) All-positive magnetic moment distribution. (f) Goal function value (equation 19a) per iteration showing the convergence.

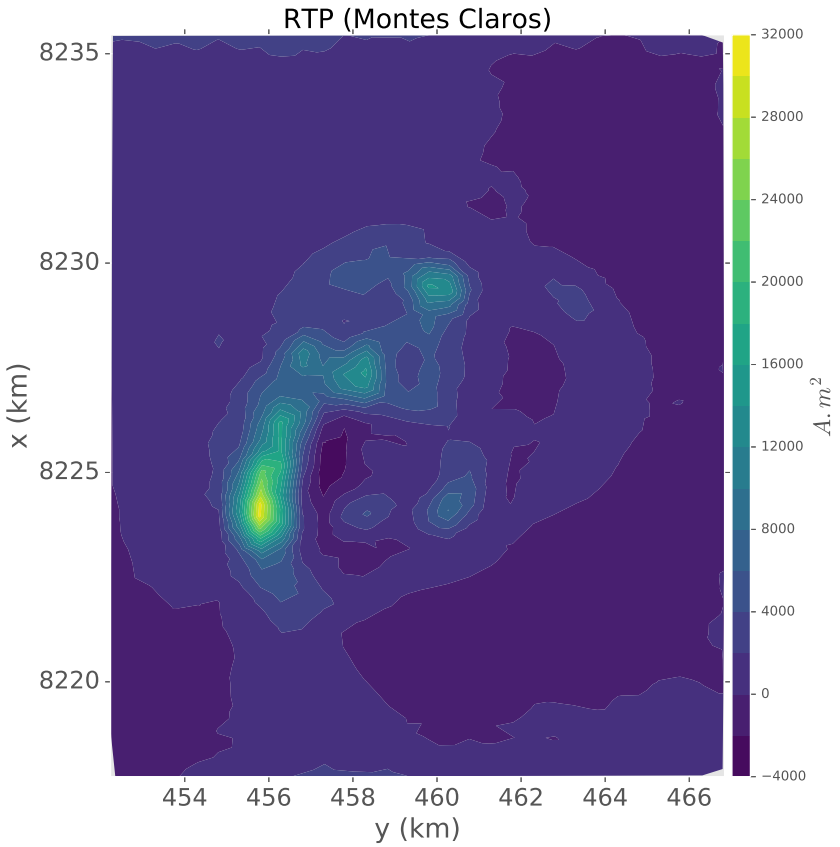

Figure 7: Application to field data ~~located in~~ complex of Montes Claros. RTP anomaly computed by using the estimated magnetization distribution shown in figure 6e.